Theoretical Analysis and Simulation of IM/DD Optical OFDM Systems

Mohammed Mossaad
McMaster University

Abstract—**A theoretical analysis of the DC-biased optical OFDM (DCO-OFDM) transmission system is presented. In particular, the effect of both the DC bias and the subsequent clipping, introduced at the transmitter, on the bit error rate (BER) performance metric is analyzed. The statistics of the nonlinear clipping noise are derived and used in our derivation of the analytical expression for the BER. Our analytical results are compared to the corresponding simulation results for different design parameters. It is shown that both analytical and simulation results are in good agreement. An additive white Gaussian noise (AWGN) channel model, commonly used with wireless optical systems, is assumed. In addition, an implicit expression for the optimal value of the DC bias as a function of the signal-to-AWGN ratio is given. As for ACO-OFDM, the BER performance of an ACO-ODM system in a multipath indoor wireless channel is obtained using simulation.**

Index Terms—**OFDM, intensity modulated direct detection, DC-biased optical OFDM, nonlinearities.**

I. Introduction

OFDM has been successfully applied to a wide variety of digital communications systems over the past years. It has been adopted in several broadband wireless communications and cable standards. Two of its major advantages in wireless communications are its robustness against multipath dispersion and ease of channel estimation in a time-varying environment. OFDM has been recently proposed for communication over optical fiber links to combat channel dispersion in fiber media which limits the data rate and length of optical fiber links. Optical OFDM solutions can be broadly divided into two types: optical OFDM using intensity modulation (IM) and optical OFDM using linear field modulation.

In this report, we focus on intensity modulation with direct detection (IM/DD) systems [1], [2], [3], [4]. Intensity modulation implies that the power of the optical signal in the fiber is proportional to the OFDM information signal to be transmitted. However, the OFDM signal is generally a complex signal and optical power must be real and positive. To solve this problem, some conditions must be imposed on the OFDM subcarriers data so that the IFFT operation produces a real signal. In an OFDM frame, if the data symbols on the subcarriers have Hermitian symmetry, then the output of the IFFT operation is real, though not necessarily positive. To make the OFDM signal positive, we add a suitable DC bias and clip the parts of the signal that are still negative, forcing them to zero [5]. Then the OFDM signal is set to modulate an optical source. At the receiver, after photodetection, the DC bias is subtracted before the FFT operation. The clipping introduces nonlinear distortion (NLD) noise. In this report, we provide a theoretical characterization of the NLD effects on the optical OFDM signal.

Nonlinear effects in non-optical OFDM systems have been extensively studied [6], [7], [8], [9]. [6] extends Bussgang's theorem (and its applications) [10], [11], [12] to bandpass memoryless nonlinearities with complex Gaussian nonzero-mean nonstationary inputs. Clipping effects have been addressed in optical OFDM systems [3], [4]. [4] compares between two types of IM/DD systems: DC-biased optical OFDM (DCO-OFDM) and asymmetrically clipped optical OFDM (ACO-OFDM). BER curves were obtained through simulations and the BER performance of the two systems was compared. No analytical formulas were obtained for the BER, however. There are studies that have obtained BER formulas in the case of coherent optical OFDM systems [13]. A recent study considered the clipping noise in an ACO-OFDM system and a formula for the BER has been derived [14]. But, to our knowledge, no previous studies have derived analytical results for BER in a DCO-OFDM system.

In this report, we derive an analytical expression for the BER of the DCO-OFDM system. The BER expression quantitatively shows how the NLD noise affects the BER performance. In particular, we compare our analytical results obtained to the simulation results in [4]. An additive white Gaussian noise (AWGN) channel is assumed. This model is used for free-space optical (FSO) communication systems where the main source of noise is the electrical receiver front-end [4]. The procedure we follow consists of tracing the signal as it is transmitted through the DCO-OFDM system up to the decision device at the receiver. Our goal is to statistically characterize the effects of the NLD noise at the input of the decision device. We prove that each data-carrying OFDM subcarrier is subject to a multiplicative scaling factor K, which is a constant independent of the subcarrier number, and an additive Gaussian noise term whose variance is dependent on the subcarrier number. We evaluate K and the NLD noise variance and use them to obtain an expression for the BER. From the BER expression, the optimal value for the DC bias is derived.

We also consider ACO-OFDM. First, a multipath indoor wireless channel model is referenced. Based on the model, the impulse response of the channel is evaluated and plotted vs. time. Then, the impulse response of the channel is used in the simulation of an ACO-OFDM system.

The remainder of this report is organized as follows. The system model is described qualitatively in Section III. A detailed mathematical analysis of the DCO-OFDM signal before clipping is carried out in Section IV. A detailed mathematical analysis of the DCO-OFDM signal at the output of the NL block is provided in Section V. The statistics of the decision variable at the receiver are derived in Section VI. Based on this statistical characterization, a formula for the bit error probability is given in Section VII, and the optimal value of the DC bias is derived. In Section VIII, we compare our analytical results with simulation results. In Section IX, the impulse response of an indoor wireless optical channel is obtained and used in the simulation of an ACO-OFDM system in Section X. Finally our conclusions are given in Section XI.

II. Literature Survey of Wireless Optical Communication Systems

In this section, we present a review of the evolution of wireless optical systems. The references are listed in chronological order as much as possible. Wireless infrared data communication was proposed for indoor applications in [15]. A recursive method for the evaluation of the impulse response of an indoor wireless optical channel with Lambertian reflectors was presented in [16]. A thorough treatment of wireless infrared communications is presented in [17]. There is an emerging interest in the use of visible LED light for data communication. This is termed visible light communications (VLC). In VLC, the LED light is used for both lighting and communications. Therefore, there are a number of constraints imposed by the lighting function. In [18], on-off keying, return-to-zero and OFDM are proposed to combat the optical path difference in an indoor VLC system using plural white LED lights. Among the applications of VLC, we mention here a traffic information system using LED traffic lights [19], the integration of VLC with power-line communication (PLC) [20], indoor three-dimensional location estimation based on LED VLC [21] and a pixelated MIMO system [22]. A proof-of-concept for VLC systems using LED lights is presented in [23]. According to the system analysis and arguments presented in [23] it is expected that VLC will be the next-generation indoor communication system.

III. System Model

The system block diagram is presented in Fig. 1. A_k^m represents the information symbols, which come from a square QAM constellation. Superscript m denotes the OFDM frame number, whereas subscript $k = 0, 1, 2, \ldots, N-1$ denotes the subcarrier number. N is the number of OFDM subcarriers. In order to suit the implementation of optical IM, the output of the IFFT should be real. It can be shown in a straightforward manner that this necessitates the following two conditions. In each OFDM frame a Hermitian symmetry condition must hold for $k \neq 0, N/2$ such that

$$A_{N-k}^m = (A_k^m)^* \tag{1}$$

In addition the 0^{th} and $(N/2)^{th}$ subcarriers are set to zero, that is,

$$A_0^m = A_{N/2}^m = 0 \tag{2}$$

For each OFDM frame, the IFFT operation is carried out to transform N complex numbers, the information symbols $A_k^m, k = 0, 1, 2, \ldots, N-1$ to N real numbers, the samples of the OFDM signal in time domain x_n^m. Thus,

$$x_n^m = \frac{1}{\sqrt{N}} \sum_{k=0}^{N-1} A_k^m e^{j2\pi kn/N} \tag{3}$$

for $n = 0, 1, ..., N-1$. It is noted here that, due to the central limit theorem, x_n^m has a Gaussian distribution, provided N is sufficiently large. Since N is typically equal to 64, 128, etc., the Gaussian assumption is valid. All samples x_n^m are real, but some samples are negative and hence not suitable for intensity modulation. To overcome this problem, a DC bias B_{DC} is added to x_n^m to produce $(x_o)_n^m$:

$$(x_o)_n^m = x_n^m + B_{DC} \tag{4}$$

We define the factor α as the ratio between B_{DC} and the RMS value of x_n^m. Thus:

$$\alpha = \frac{B_{DC}}{\sqrt{E\left[(x_n^m)^2\right]}} \tag{5}$$

We define the DC bias in dB, $B_{DC}(\text{dB})$, as:

$$B_{DC}(\text{dB}) = 10\log_{10}\left[\frac{E\left[\left[(x_o)_n^m\right]^2\right]}{E\left[(x_n^m)^2\right]}\right] = 10\log_{10}\left(\alpha^2+1\right) \tag{6}$$

Some samples $(x_o)_n^m$ may still be negative. Therefore, the samples $(x_o)_n^m$ are clipped, that is, all negative samples are set to zero. At the receiver, the DC bias is subtracted before the samples are fed to the FFT block. But the clipping causes loss of information in the sense that, ignoring all other sources of noise and error, the recovered symbols at the receiver will be noisy versions of those transmitted due to clipping. We develop an analytical approach to characterize this noise component and its effect on BER performance. We also emphasize the effect of the DC bias on the clipping noise. Clearly, the larger the bias, the smaller the clipping noise. But a large bias would mean increased transmission power. So there is a trade-off between power and BER performance. Thus, the value of B_{DC} should be optimized according to system requirements. It is noted that the input sample suffers clipping only when its value is less than $-B_{DC}$. The OFDM signal is then used to modulate an optical source which is assumed to be ideal, achieving a linear transformation between the input signal and the output optical power. An AWGN channel is assumed. At the receiver, after (ideal) photodetection, the signal $v(t)$ is sampled and the samples v_n^m are fed to the FFT block which is followed by the symbol detector.

IV. Mathematical Analysis of the DCO-OFDM Signal before Clipping

In this section, we provide a complete statistical description of the DCO-OFDM signal at the input of the clipping device. It is necessary to obtain the input statistics, in order to derive the output statistics and the statistics of the decision variable at the receiver in Section VI.

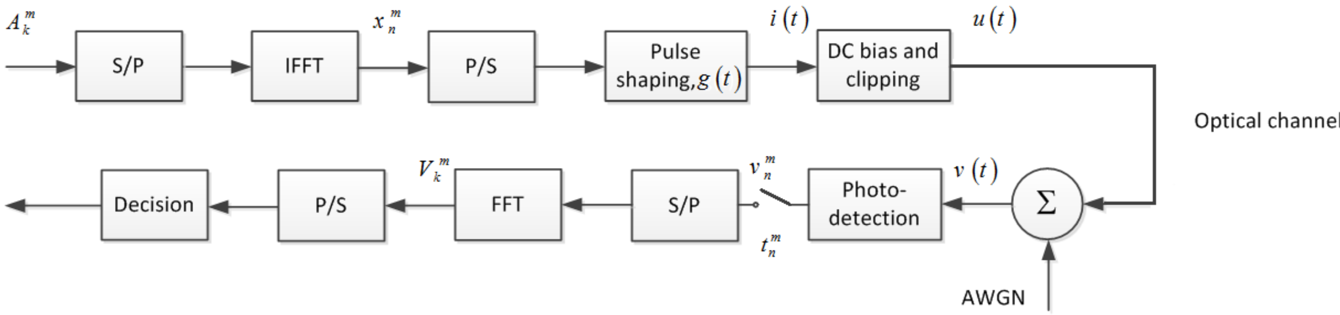

Fig. 1. System block diagram.

The DCO-OFDM signal, before clipping, is given by:

$$x(t) = \sum_{m=-\infty}^{\infty} \sum_{n=0}^{N-1} x_n^m g(t - nT - mNT) \tag{7}$$

where x_n^m is given in (3). T is the channel symbol time, $g(t)$ is the pulse shaping function introduced when converting the signal from digital to analog after IFFT. $g(t)$ is chosen to be limited in time, that is, $g(t) = 0$ for $|t| > T/2$. For simplicity, we choose $g(t)$ to be a rectangular pulse of unity amplitude and a duration of T, centered at $t = 0$. Therefore, $g(t)$ can be expressed as:

$$g(t) = \Pi(t) = \begin{cases} 1 & \text{for } -T/2 \le t < T/2 \\ 0 & \text{for } t < -T/2 \text{ or } t \ge T/2 \end{cases} \tag{8}$$

Symbols A_k^m belong to an alphabet $\mathcal{A}$ of M elements, which depend on the modulation format, and have the same probability. In order for $x(t)$ to be real, conjugate symmetry conditions are imposed on the subcarrier data and the 0^{th} and $(N/2)^{\text{th}}$ subcarriers are set to zero as described by Eqs. (1) and (2). Considering square QAM constellations, A_k^m can be written in terms of its real and imaginary parts:

$$A_k^m = X_k^m + jY_k^m \tag{9}$$

where the real and imaginary parts; X_k and Y_k, respectively; are zero-mean random variables with

$$E\left[(X_k^m)^2\right] = E\left[(Y_k^m)^2\right] \tag{10}$$

and

$$E\left[(X_k^m)^2\right] + E\left[(Y_k^m)^2\right] = P \quad k \ne 0, N/2 \tag{11}$$

where P is the average energy per symbol in the constellation. It follows from (10) and (11) that:

$$E\left[(X_k^m)^2\right] = E\left[(Y_k^m)^2\right] = P/2 \quad k \ne 0, N/2 \tag{12}$$

Also, for a square QAM constellation, assuming all information symbols are sent with equal probabiliy:

$$E\left[X_k^m Y_k^m\right] = 0 \tag{13}$$

More generally,

$$E\left[X_k^m Y_h^l\right] = 0 \tag{14}$$

for every $k, h = 0, 1, ..., N-1$ and for every m and l. It follows from the conjugate symmetry condition that:

$$E\left[X_k^m X_{N-k}^l\right] = \begin{cases} P/2 & \text{for } m = l \text{ and } k \ne 0, N/2 \\ 0 & \text{otherwise} \end{cases} \tag{15}$$

and

$$E\left[Y_k^m Y_{N-k}^l\right] = \begin{cases} -P/2 & \text{for } m = l \text{ and } k \ne 0, N/2 \\ 0 & \text{otherwise} \end{cases} \tag{16}$$

Based on Eqs. (10)-(16), the following relations hold for every $k, h = 0, 1, ..., N-1$ and for every m and l:

$$E\left[A_k^m\right] = 0 \tag{17}$$

$$E\left[A_k^m A_h^l\right] = \begin{cases} P & \text{for } m = l \text{ and } h = N-k, k \ne 0, N/2 \\ 0 & \text{otherwise} \end{cases} \tag{18}$$

$$E\left[A_k^m \left(A_h^l\right)^*\right] = \begin{cases} P & \text{for } m = l \text{ and } h = k, k \ne 0, N/2 \\ 0 & \text{otherwise} \end{cases} \tag{19}$$

The mean of the sample x_n^m is:

$$\beta_x = E\left[x_n^m\right] = \frac{1}{\sqrt{N}} \sum_{k=0}^{N-1} E\left[A_k^m\right] e^{j2\pi kn/N} = 0 \tag{20}$$

where (17) was used. The mean square value of the sample x_n^m is computed as follows:

$$\begin{aligned} \sigma_x^2 = E\left[(x_n^m)^2\right] &= \frac{1}{N} \sum_{k=0}^{N-1} \sum_{h=0}^{N-1} E\left[A_k^m A_h^m\right] e^{j2\pi(k+h)n/N} \\ &= \frac{1}{N} \sum_{\substack{k=1 \\ k \ne N/2}}^{N-1} P e^{j2\pi(k+(N-k))n/N} \\ &= \left(1 - \frac{2}{N}\right) P \end{aligned} \tag{21}$$

where the second line follows from (18) and the factor $\frac{2}{N}$ in the last line accounts for the two subcarriers set to zero. The covariance of two samples of $x(t)$, x_n^m and x_p^m, taken at $t_n^m = nT + mNT$ and $t_p^m = pT + mNT$, respectively, is given by:

$$\begin{aligned}\mu(n,p) &= E[x_n^m x_p^m] \\ &= \frac{1}{N}\sum_{k=0}^{N-1}\sum_{h=0}^{N-1} E\left[A_k^m A_h^m\right] e^{j2\pi(kn+hp)/N} \\ &= \frac{1}{N}\sum_{\substack{k=1\\k\neq N/2}}^{N-1} P e^{j2\pi[kn+(N-k)p]/N} \\ &= \frac{P}{N}\sum_{\substack{k=1\\k\neq N/2}}^{N-1} e^{j2\pi k(n-p)/N} \\ &= \frac{P}{N}\sum_{k=1}^{\frac{N}{2}-1}\left[e^{j2\pi k(n-p)/N} + e^{j2\pi (N-k)(n-p)/N}\right] \\ &= \begin{cases}\left(1-\frac{2}{N}\right)P & \text{for } n=p \\ -\frac{2}{N}P & \text{for } n-p \text{ even } (n\neq p) \\ 0 & \text{for } n-p \text{ odd}\end{cases} \end{aligned} \tag{22}$$

where the third equality follows from (18). Eqs. (20), (21), (22), and the Gaussian assumption provide a complete statistacal description of the random signal $x(t)$ and its samples x_n^m up to the second order statistics. The correlation coefficient of the two samples x_n^m and x_p^m is given by:

$$\begin{aligned}\rho(n,p) &= \frac{\mu(n,p)}{\sigma_x^2} \\ &= \begin{cases}1 & \text{for } n=p \\ -\left(\frac{N}{2}-1\right)^{-1} & \text{for } n-p \text{ even, and } n\neq p \\ 0 & \text{for } n-p \text{ odd}\end{cases}\end{aligned} \tag{23}$$

In the next section, we consider the effects of the nonlinear clipping device on the statistics of the DCO-OFDM signal.

V. Mathematical Analysis of the DCO-OFDM Signal at the Output of the Nonlinear Block

We focus our attention on the output of the nonlinear block $u(t)$. Our goal is to represent this output as

$$u(t) = F[x(t)] = Kx(t) + d(t) \tag{24}$$

where $F(.)$ is the nonlinear clipping function, $d(t)$ is a suitably introduced additive noise term, and K is a deterministic function. The cross-correlation between the input to the nonlinear clipping device $x(t)$ delayed by τ and the output $u(t)$ is evaluated using their joint statistics as follows:

$$E[u(t)x(t+\tau)] = E[F[x(t)]x(t+\tau)] \tag{25}$$

Denote $x(t)$ as x_1 and $x(t+\tau)$ as x_2 for simplicity. Thus, we can write:

$$\begin{aligned}E[u(t)x(t+\tau)] &= E[F(x_1)x_2] \\ &= \int_{-\infty}^{\infty}\int_{-\infty}^{\infty} F(x_1)x_2 f_{X_1X_2}(x_1,x_2)dx_1dx_2\end{aligned} \tag{26}$$

x_1 and x_2 are jointly Gaussian RVs with zero means. Each has a variance of σ_x^2. Let $\mu = E[x_1x_2]$ be the covariance of x_1 and x_2 and $\rho = \frac{\mu}{\sigma_x^2}$ be their correlation coefficient. The bivariate Gaussian distribution is defined in terms of these parameters:

$$f_{X_1X_2}(x_1,x_2) = \frac{1}{2\pi\sigma_x^2\sqrt{1-\rho^2}}\exp\left[-\frac{x_1^2+x_2^2-2\rho x_1x_2}{2\sigma_x^2(1-\rho^2)}\right] \tag{27}$$

The nonlinear clipping function is given by:

$$F(x) = \begin{cases}-B_{DC} & \text{for } x < -B_{DC} \\ x & \text{for } x \geq -B_{DC}\end{cases} \tag{28}$$

Substituting from (28) into (26), we get:

$$\begin{aligned}&E[F(x_1)x_2] \\ &= -B_{DC}\int_{x_1=-\infty}^{-B_{DC}}\int_{x_2=-\infty}^{\infty} x_2 f_{X_1X_2}(x_1,x_2)dx_1dx_2 \\ &\quad + \int_{-B_{DC}}^{\infty}\int_{-\infty}^{\infty} x_1x_2 f_{X_1X_2}(x_1,x_2)dx_1dx_2\end{aligned} \tag{29}$$

Carrying out the integrations, we get:

$$\begin{aligned}E\left[F(x_1)x_2\right] =& \rho\sigma_x^2\left[\frac{B_{DC}}{\sqrt{2\pi}\sigma_x}\exp\left(-\frac{B_{DC}^2}{2\sigma_x^2}\right)\right. \\ &\left. + \frac{1}{\sqrt{\pi}}\gamma\left(\frac{3}{2},\frac{B_{DC}^2}{2\sigma_x^2}\right) + \frac{1}{2}\right]\end{aligned} \tag{30}$$

where $\gamma(s,x) = \int_0^x t^{s-1}e^{-t}dt = 2\int_0^{\sqrt{x}} t^{2s-1}e^{-t^2}dt$ is the lower incomplete Gamma function. But $\rho\sigma_x^2 = E[x_1x_2] = E[x(t)x(t+\tau)] = \mu$. Thus, (30) can be written as:

$$\begin{aligned}E[F(x_1)x_2] &= \left[\frac{B_{DC}}{\sqrt{2\pi}\sigma_x}\exp\left(-\frac{B_{DC}^2}{2\sigma_x^2}\right)\right. \\ &\quad \left. + \frac{1}{\sqrt{\pi}}\gamma\left(\frac{3}{2},\frac{B_{DC}^2}{2\sigma_x^2}\right) + \frac{1}{2}\right]\mu \\ &= KE[x_1x_2]\end{aligned} \tag{31}$$

where

$$K = \frac{B_{DC}}{\sqrt{2\pi}\sigma_x}\exp\left(-\frac{B_{DC}^2}{2\sigma_x^2}\right) + \frac{1}{\sqrt{\pi}}\gamma\left(\frac{3}{2},\frac{B_{DC}^2}{2\sigma_x^2}\right) + \frac{1}{2} \tag{32}$$

From (31), $F(x_1)$ can be expressed as:

$$F(x_1) = Kx_1 + d_1 \tag{33}$$

or

$$F[x(t)] = Kx(t) + d(t) \tag{34}$$

where $d_1 = d(t)$ is an additive noise term uncorrelated with $x_2 = x(t+\tau)$. That is:

$$E[d_1x_2] = E[d(t)x(t+\tau)] = 0 \tag{35}$$

The mean of $u(t)$ is computed as follows:

$$\begin{aligned}E[u(t)] =& E[F[x(t)]] = E[F(x_1)] = \int_{-\infty}^{\infty} F[x_1]f_{X_1}(x_1)dx_1 \\ =& \frac{1}{\sqrt{2\pi}\sigma_x}\int_{-\infty}^{-B_{DC}} -B_{DC}\exp\left(-\frac{x_1^2}{2\sigma_x^2}\right)dx_1 \\ &+ \frac{1}{\sqrt{2\pi}\sigma_x}\int_{-B_{DC}}^{\infty} x_1\exp\left(-\frac{x_1^2}{2\sigma_x^2}\right)dx_1 \\ =& \frac{\sigma_x}{\sqrt{2\pi}}\exp\left(-\frac{B_{DC}^2}{2\sigma_x^2}\right) - \frac{1}{2}B_{DC}\operatorname{erfc}\left(\frac{B_{DC}}{\sqrt{2}\sigma_x}\right)\end{aligned} \tag{36}$$

From (33), $E[u(t)] = E[F(x_1)] = KE[x_1] + E[d_1] = E[d_1]$ as $E[x_1] = \beta_x = 0$. Therefore, the mean, β_d, of the noise term $d(t)$ is:

$$\beta_d = E[d(t)] = E[d_1] = \frac{\sigma_x}{\sqrt{2\pi}} \exp\left(-\frac{B_{DC}^2}{2\sigma_x^2}\right) - \frac{1}{2} B_{DC} \operatorname{erfc}\left(\frac{B_{DC}}{\sqrt{2}\sigma_x}\right) \tag{37}$$

The representation of the output of the nonlinear clipping device given by (34) indicates that the effect of the clipping on the input DCO-OFDM signal is a scaling factor K and an additive noise term $d(t)$. For the probability of error to be properly evaluated, the effects of K and $d(t)$ on the input to the decision device at the receiver should be carefully considered. This is treated in the next section.

VI. Statistical Characterization of the Decision Variables at the Receiver

Assuming an additive white Gaussian noise (AWGN) channel, the signal before the sampling at the receiver is given by:

$$v(t) = u(t) + w(t) = Kx(t) + d(t) + w(t) \tag{38}$$

where $w(t)$ is a zero-mean white Gaussian noise signal having a single-sided power spectral density of N_0. Since the main noise source is electrical rather than optical, the AWGN is bipolar, rather than unipolar. Sampling at $t_n^m = nT + mNT$, we get the samples that are fed to the FFT operation:

$$v_n^m = u_n^m + w_n^m = Kx_n^m + d_n^m + w_n^m \tag{39}$$

The FFT output is, hence:

$$\begin{aligned} V_k^m =& \frac{1}{\sqrt{N}} \sum_{n=0}^{N-1} v_n^m e^{-j2\pi kn/N} \\ =& K\left[\frac{1}{\sqrt{N}} \sum_{n=0}^{N-1} x_n^m e^{-j2\pi kn/N}\right] \\ &+ \frac{1}{\sqrt{N}} \sum_{n=0}^{N-1} d_n^m e^{-j2\pi kn/N} \\ &+ \frac{1}{\sqrt{N}} \sum_{n=0}^{N-1} w_n^m e^{-j2\pi kn/N} \\ =& KA_k^m + D_k^m + W_k^m \end{aligned} \tag{40}$$

where

$$D_k^m = \frac{1}{\sqrt{N}} \sum_{n=0}^{N-1} d_n^m e^{-j2\pi kn/N} \tag{41}$$

is the clipping noise component at the k^{th} subcarrier at the output of the FFT block and

$$W_k^m = \frac{1}{\sqrt{N}} \sum_{n=0}^{N-1} w_n^m e^{-j2\pi kn/N} \tag{42}$$

is the AWGN component. The variance of W_k^m, σ_W^2, is computed as follows:

$$\begin{aligned} \sigma_W^2 &= E[W_k^m (W_k^m)^*] \\ &= \frac{1}{N} \sum_{n=0}^{N-1} \sum_{p=0}^{N-1} E[w_n^m w_p^m] e^{-j2\pi k(n-p)/N} \\ &= \frac{1}{N} \times NE\left[\left(w_n^m\right)^2\right] \\ &= \sigma_w^2 \end{aligned} \tag{43}$$

where we have used the fact that $E[w_n^m w_p^m] = 0$ for $n \neq p$ as we have white noise (uncorrelated from sample to sample). Here $\sigma_w^2 = E\left[\left(w_n^m\right)^2\right] = N_0$ is the variance of the AWGN sample w_n^m. To obtain a formula for the BER, we also have to evaluate σ_D^2, the variance of D_k^m. First, we compute the mean of D_k^m:

$$\begin{aligned} E[D_k^m] &= \frac{1}{\sqrt{N}} \sum_{n=0}^{N-1} E[d_n^m] e^{-j2\pi kn/N} \\ &= \begin{cases} \sqrt{N}\beta_d & \text{for } k = 0 \\ 0 & \text{for } k = 1, 2, \ldots, N-1 \end{cases} \end{aligned} \tag{44}$$

Thus, only the NLD noise component affecting the 0^{th} subcarrier (that does not carry any data symbols) has a non-zero mean. We then proceed by computing the mean-square value of D_k^m:

$$\begin{aligned} & E\left[\left|D_k^m\right|^2\right] = E\left[D_k^m (D_k^m)^*\right] \\ =& \frac{1}{N} \sum_{n=0}^{N-1} \sum_{p=0}^{N-1} E[d_n^m d_p^m] e^{-j2\pi k(n-p)/N} \\ =& E\left[\left(d_n^m\right)^2\right] \\ &+ \frac{1}{N} E\left[d_n^m d_p^m\right]_{(n-p \text{ odd})} \sum_{n=0}^{N-1} \sum_{\substack{p=0 \\ n-p \text{ odd}}}^{N-1} e^{-j2\pi k(n-p)/N} \\ &+ \frac{1}{N} E\left[d_n^m d_p^m\right]_{\left(\substack{n-p \text{ even} \\ n \neq p}\right)} \sum_{n=0}^{N-1} \sum_{\substack{p=0 \\ n-p \text{ even} \\ n \neq p}}^{N-1} e^{-j2\pi k(n-p)/N} \end{aligned} \tag{45}$$

It can be easily shown that, for $k \neq 0, N/2$:

$$\sum_{n=0}^{N-1} \sum_{\substack{p=0 \\ n-p \text{ odd}}}^{N-1} e^{-j2\pi k(n-p)/N} = 0, \tag{46}$$

and

$$\sum_{n=0}^{N-1} \sum_{\substack{p=0 \\ n-p \text{ even} \\ n \neq p}}^{N-1} e^{-j2\pi k(n-p)/N} = -N. \tag{47}$$

Substituting from (46) and (47) into (45), we get:

$$E\left[\left|D_k^m\right|^2\right] = E\left[\left(d_n^m\right)^2\right] - E\left[d_n^m d_p^m\right]_{\left(\substack{n-p \text{ even} \\ n \neq p}\right)} \tag{48}$$

where $E\left[d_n^m d_p^m\right]_{\binom{n-p \text{ even}}{n\neq p}}$ is to be evaluated using a correlation coefficient $\rho(n,p) = -\left(\frac{N}{2}-1\right)^{-1} = \rho'$ according to (23).

The first term of the right-hand side of (48) is:

$$E\left[(d_n^m)^2\right] = E\left[(u_n^m - Kx_n^m)^2\right] = E\left[(u_n^m)^2\right] + K^2 E\left[(x_n^m)^2\right] - 2KE[u_n^m x_n^m] \tag{49}$$

where

$$E\left[(x_n^m)^2\right] = \sigma_x^2, \tag{50}$$

$$\begin{aligned}E\left[(u_n^m)^2\right] =& E\left[[F(x_1)]^2\right] \\ =& \int_{-\infty}^{-B_{DC}} (-B_{DC})^2 f_{X_1}(x_1)dx_1 \\ &+ \int_{-B_{DC}}^{\infty} x_1^2 f_{X_1}(x_1)dx_1 \\ =& \frac{B_{DC}^2}{\sqrt{2\pi}\sigma_x}\int_{-\infty}^{-B_{DC}} \exp\left(-\frac{x_1^2}{2\sigma_x^2}\right)dx_1 \\ &+ \frac{1}{\sqrt{2\pi}\sigma_x}\int_{-B_{DC}}^{\infty} x_1^2 \exp\left(-\frac{x_1^2}{2\sigma_x^2}\right)dx_1 \\ =& \frac{1}{2}B_{DC}^2 \text{erfc}\left(\frac{B_{DC}}{\sqrt{2}\sigma_x}\right) \\ &+ \sigma_x^2\left[\frac{1}{2} + \frac{1}{\sqrt{\pi}}\gamma\left(\frac{3}{2}, \frac{B_{DC}^2}{2\sigma_x^2}\right)\right],\end{aligned} \tag{51}$$

and

$$\begin{aligned}E[u_n^m x_n^m] =& E[F(x_1)x_1] \\ =& \int_{-\infty}^{-B_{DC}} (-B_{DC}x_1) f_{X_1}(x_1)dx_1 \\ &+ \int_{-B_{DC}}^{\infty} x_1^2 f_{X_1}(x_1)dx_1 \\ =& \frac{-B_{DC}}{\sqrt{2\pi}\sigma_x}\int_{-\infty}^{-B_{DC}} x_1 \exp\left(-\frac{x_1^2}{2\sigma_x^2}\right)dx_1 \\ &+ \frac{1}{\sqrt{2\pi}\sigma_x}\int_{-B_{DC}}^{\infty} x_1^2 \exp\left(-\frac{x_1^2}{2\sigma_x^2}\right)dx_1 \\ =& \sigma_x^2\left[\frac{B_{DC}}{\sqrt{2\pi}\sigma_x}\exp\left(-\frac{B_{DC}^2}{2\sigma_x^2}\right)\right. \\ &\left.+ \frac{1}{\sqrt{\pi}}\gamma\left(\frac{3}{2}, \frac{B_{DC}^2}{2\sigma_x^2}\right) + \frac{1}{2}\right] \\ =& K\sigma_x^2.\end{aligned} \tag{52}$$

Substituting (50)-(52) into (49), we get, after a few algebraic manipulations:

$$\begin{aligned}E\left[(d_n^m)^2\right] =& \frac{1}{2}B_{DC}^2 \text{erfc}\left(\frac{B_{DC}}{\sqrt{2}\sigma_x}\right) \\ &+ \sigma_x^2\left[\frac{1}{\sqrt{\pi}}\gamma\left(\frac{3}{2}, \frac{B_{DC}^2}{2\sigma_x^2}\right) + \frac{1}{2} - K^2\right]\end{aligned} \tag{53}$$

Turning our attention to the second term of the right-hand side of (48), we have:

$$\begin{aligned}E[d_n^m d_p^m] &= E[(u_n^m - Kx_n^m)d_p^m] = E[u_n^m d_p^m] \\ &= E[u_n^m(u_p^m - Kx_p^m)] = E[u_n^m u_p^m] - KE[u_n^m x_p^m] \\ &= E[u_n^m u_p^m] - KE[(Kx_n^m + d_n^m)x_p^m] \\ &= E[u_n^m u_p^m] - K^2 E[x_n^m x_p^m]\end{aligned} \tag{54}$$

where

$$E[x_n^m x_p^m] = \mu = \rho'\sigma_x^2, \tag{55}$$

and

$$\begin{aligned}&E[u_n^m u_p^m] = E[F(x_1)F(x_2)] \\ =& B_{DC}^2 \int_{x_1=-\infty}^{-B_{DC}}\int_{x_2=-\infty}^{-B_{DC}} f_{X_1X_2}(x_1,x_2)dx_1dx_2 \\ &- B_{DC}\int_{x_1=-\infty}^{-B_{DC}}\int_{x_2=-B_{DC}}^{\infty} x_2 f_{X_1X_2}(x_1,x_2)dx_1dx_2 \\ &- B_{DC}\int_{x_1=-B_{DC}}^{\infty}\int_{x_2=-\infty}^{-B_{DC}} x_1 f_{X_1X_2}(x_1,x_2)dx_1dx_2 \\ &+ \int_{-B_{DC}}^{\infty}\int_{-B_{DC}}^{\infty} x_1x_2 f_{X_1X_2}(x_1,x_2)dx_1dx_2 \\ =& \frac{B_{DC}^2}{2\sigma_x\sqrt{2\pi}}\int_{-\infty}^{-B_{DC}} \text{erfc}\left[\frac{\rho' x + B_{DC}}{\sigma_x\sqrt{2\left(1-(\rho')^2\right)}}\right] e^{-\frac{x^2}{2\sigma_x^2}}dx \\ &+ \rho'\left(1-(\rho')^2\right)\frac{B_{DC}\sigma_x}{\sqrt{2\pi}} e^{-\frac{B_{DC}^2}{2\sigma_x^2}} \\ &\times\left[1 - \frac{1}{2}\text{erfc}\left(\frac{B_{DC}}{\sqrt{2}\sigma_x}\sqrt{\frac{1-\rho'}{1+\rho'}}\right)\right] \\ &- \frac{B_{DC}\sigma_x}{\sqrt{2\pi}} e^{-\frac{B_{DC}^2}{2\sigma_x^2}}\text{erfc}\left(\frac{B_{DC}}{\sqrt{2}\sigma_x}\sqrt{\frac{1-\rho'}{1+\rho'}}\right) \\ &+ \left(1+(\rho')^2\right)\sqrt{1-(\rho')^2}\frac{\sigma_x^2}{2\pi}\exp\left[-\frac{B_{DC}^2}{\sigma_x^2(1+\rho')}\right] \\ &+ \rho'\frac{\sigma_x^2}{2}\left[1 - \frac{1}{2}\text{erfc}\left(\frac{B_{DC}}{\sqrt{2}\sigma_x}\right)\right] \\ &+ \rho'\frac{\sigma_x}{\sqrt{2\pi}}\int_{-B_{DC}}^{\infty}\gamma\left[\frac{3}{2}, \frac{(\rho' x + B_{DC})^2}{2\sigma_x^2\left(1-(\rho')^2\right)}\right] e^{-\frac{x^2}{2\sigma_x^2}}dx.\end{aligned} \tag{56}$$

Substituting from (55) into (54), we get:

$$E[d_n^m d_p^m] = E[u_n^m u_p^m] - \rho' K^2 \sigma_x^2 \tag{57}$$

Noting that, for $k \neq 0$, the variance of D_k^m:

$$\sigma_D^2 = E\left[|D_k^m|^2\right] - E\left[D_k^m\right]E\left[(D_k^m)^*\right] = E\left[|D_k^m|^2\right] \tag{58}$$

due to (44), then substituting from (53) and (57) into (48), we get:

$$\begin{aligned}\sigma_D^2 =& E\left[|D_k^m|^2\right] = \frac{1}{2}B_{DC}^2\text{erfc}\left(\frac{B_{DC}}{\sqrt{2}\sigma_x}\right) \\ &+ \sigma_x^2\left[\frac{1}{\sqrt{\pi}}\gamma\left(\frac{3}{2}, \frac{B_{DC}^2}{2\sigma_x^2}\right) + \frac{1}{2} - (1-\rho')K^2\right]' \\ &- E\left[u_n^m u_p^m\right]\end{aligned} \tag{59}$$

The variance of the noise term D_k^m affecting the k^{th} subcarrier represents the energy of the noise term. Applying the central limit theorem to (41), the pdf of D_k^m approaches a Gaussian pdf, and the approximation gets closer to the true pdf as N increases. This approximation causes a discrepancy between the BER simulation results and our derived BER formula which assumes the nonlinear clipping noise is Gaussian. It is noticeable only in the high SNR regime where the nonlinear clipping noise dominates over the AWGN.

VII. Evaluation of Error Probability

The decision variable at the input of the decision device is given by:

$$V_k^m = KA_k^m + D_k^m + W_k^m \tag{60}$$

We divide by K so that the received constellation is a noisy, but not a scaled version of the transmitted constellation. The input to the decision device becomes:

$$(V_k^m)' = A_k^m + \frac{D_k^m}{K} + \frac{W_k^m}{K} \tag{61}$$

The symbol-error probability P_e can be evaluated by considering error probabilities conditioned on the transmission of each symbol of the modulation alphabet, as follows

$$P_e = \frac{1}{M}\sum_{A\in\mathcal{A}}\left[1 - \text{Prob}\left\{(V_k^m)' \in S_A \mid A_k^m = A\right\}\right] \tag{62}$$

where S_A is the decision region for symbol A. It requires the statistical characterization of the decision variable V_k^m. Starting from the expression of the decision variable at the input of the decision device given in (60), we can evaluate the bit-error probability as a function of the modulation format and the signal-to-total-noise ratio

$$S/N = \frac{\sigma_x^2}{(\sigma_D^2/K^2) + (\sigma_W^2/K^2)} = \frac{K^2\sigma_x^2}{\sigma_D^2 + \sigma_W^2} \tag{63}$$

An expression of the bit-error probability can be derived for several modulation formats. In this report, we specialize the derivation for square M-QAM constellations. In this case, the probability of error is given by [24]:

$$\begin{aligned} P_e &= \frac{2\left(\sqrt{M}-1\right)}{\sqrt{M}\log_2 M}\text{erfc}\left(\sqrt{\frac{3\,(S/N)}{2\,(M-1)}}\right) \\ &= \frac{2\left(\sqrt{M}-1\right)}{\sqrt{M}\log_2 M}\text{erfc}\left(\sqrt{\frac{3K^2\sigma_x^2}{2\,(M-1)\,(\sigma_D^2+\sigma_W^2)}}\right) \end{aligned} \tag{64}$$

The bit-error probability has an irreducible floor

$$P_{e_{\text{floor}}} = \frac{2\left(\sqrt{M}-1\right)}{\sqrt{M}\log_2 M}\text{erfc}\left(\frac{K\sigma_x}{\sigma_D}\sqrt{\frac{3}{2\,(M-1)}}\right) \tag{65}$$

which depends on the signal-to-NLD-noise ratio K^2/σ_D^2. In the next section, we plot the bit-error probability expression obtained above versus E_b/N_0 (where E_b is the electrical energy per bit) and we compare to simulation results.

We now explain the procedure to obtain the optimal DC bias. Our first goal is to express the AWGN variance σ_w^2 as a function of the DC bias B_{DC}. This is necessary for deriving an expression for the optimal DC bias, since all parameters affecting the probability of error must be expressed as a function of the DC bias. The signal-to-AWGN ratio per subcarrier $\left(\sigma_x^2 + B_{DC}^2\right)/N_0$ equals the signal-to-AWGN ratio per bit E_b/N_0 times the number of bits per symbol $\log_2 M$. Thus, we have:

$$\frac{\sigma_x^2 + B_{DC}^2}{N_0} = \frac{E_b}{N_0}\log_2 M \tag{66}$$

from which

$$N_0 = \sigma_w^2 = \frac{\sigma_x^2 + B_{DC}^2}{10^{[E_b/N_0(\text{dB})]/10}\log_2 M} \tag{67}$$

Next, the optimal DC bias B_o can be found by maximizing the signal-to-total-noise ratio S/N given by (63) with respect to B_{DC}. Differentiating with respect to B_{DC} and equating to zero, we get:

$$\left[2\frac{\partial K}{\partial B_{DC}}\left(\sigma_D^2+\sigma_w^2\right) - K\left(\frac{\partial\sigma_D^2}{\partial B_{DC}} + \frac{\partial\sigma_w^2}{\partial B_{DC}}\right)\right]_{B_{DC}=B_o} = 0 \tag{68}$$

Expressing K, σ_D^2, and σ_w^2 as functions of B_{DC} using (32), (56), (59), and (67), making the approximation $\rho' \approx 0$ to simplify the result, and carrying out the differentiations, we obtain the following implicit expression for the optimal DC bias B_o:

$$\begin{aligned} &\frac{B_o}{2\pi}\exp\left(-\frac{B_o^2}{\sigma_x^2}\right)\text{erfc}\left(\frac{B_o}{\sqrt{2}\sigma_x}\right) - \frac{\sigma_x}{\pi\sqrt{2\pi}}\exp\left(-\frac{3B_o^2}{2\sigma_x^2}\right) \\ &+ \sqrt{\frac{2}{\pi}}\frac{\sigma_x}{10^{[E_b/N_0(\text{dB})]/10}\log_2 M}\exp\left(-\frac{B_o^2}{2\sigma_x^2}\right) \\ &+ \left[\sqrt{\frac{2}{\pi}}\sigma_x\exp\left(-\frac{B_o^2}{2\sigma_x^2}\right) - B_o\text{erfc}\left(\frac{B_o}{\sqrt{2}\sigma_x}\right)\right. \\ &+ \frac{B_o}{2}\text{erfc}^2\left(\frac{B_o}{\sqrt{2}\sigma_x}\right) - \frac{\sigma_x}{\sqrt{2\pi}}\exp\left(-\frac{B_o^2}{2\sigma_x^2}\right)\text{erfc}\left(\frac{B_o}{\sqrt{2}\sigma_x}\right) \\ &\left. - \frac{2B_o}{10^{[E_b/N_0(\text{dB})]/10}\log_2 M}\right]\left[\frac{1}{\sqrt{\pi}}\gamma\left(\frac{3}{2},\frac{B_o^2}{2\sigma_x^2}\right) + \frac{1}{2}\right] = 0 \end{aligned} \tag{69}$$

Eq. (69) can be solved numerically for B_o. The optimal DC bias B_o is a function of the signal-to-AWGN ratio per bit E_b/N_0 and the square QAM constellation size M. In the next section, the expression for B_o is compared to simulation results.

VIII. Numerical Results

Results were obtained for $N = 2,048$ subcarriers, with 4-QAM, 16-QAM, and 64-QAM constellations. Linear field modulation bipolar 4-QAM (where Hermitian symmetry is not imposed and no DC bias and clipping are needed) is included for reference. A DC bias of 7 dB is used. This is the same value used for the simulation in [4]. We reproduce the simulation results in [4] and compare them to the analytical BER expression given by (64) that we derived in the previous sections. The results are shown in Fig. 2. The analytical expression derived for the bit-error probability is plotted in red while the simulation results are shown in black. The results show close agreement. A small discrepancy arises,

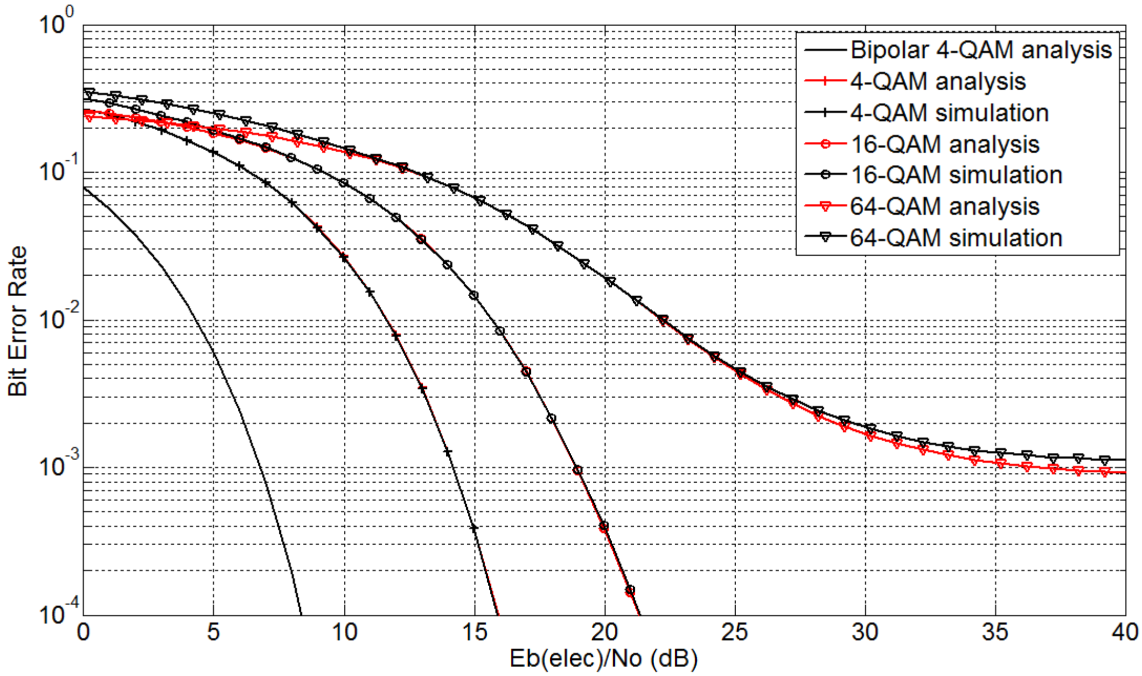

Fig. 2. BER versus SNR E_b/N_0 (dB) curve: analytical expression in red and simulation results in blue.

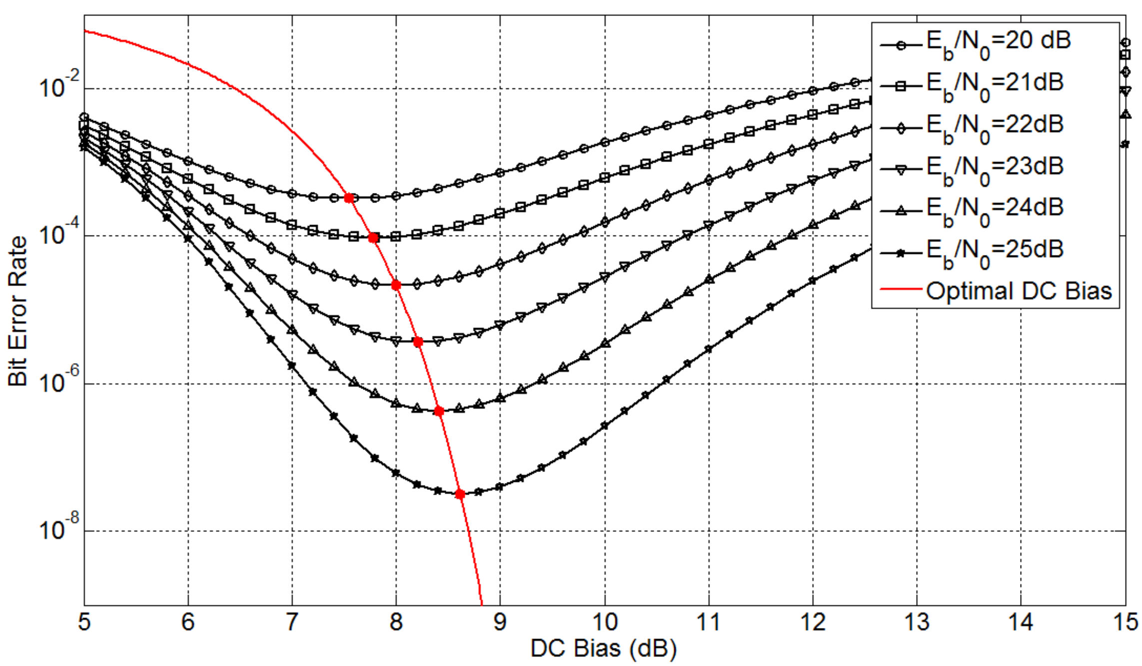

Fig. 3. Plot of the simulated BER versus the DC Bias in dB with 16-QAM and different values of E_b/N_0 (dB). Also plotted for comparison is the analytical optimal DC bias and the corresponding BER.

howerver, for small E_b/N_0 values. This is due to the fact that the BER formula used ignores symbol errors involving non-adjacent QAM symbols. Each of such errors corresponds to more than one bit in error assuming Gray coding is used. At low E_b/N_0 values, these errors are significant, but as E_b/N_0 increases beyond a few dBs, they can be safely ignored. Another small discrepancy occurs between the analytical BER formula and the simulation results for large E_b/N_0 values, which is noticeable in the 64-QAM case as is clear in Fig. 2. This is due to the the assumption used in the derivation of our BER formula, that D_k^m has a Gaussian pdf. This discrepancy almost disappears if we simulate for $N = 16,384 = 2^{14}$. In this case, applying the CLT, the Gaussian pdf is very close to the true pdf, as N is very large.

In Fig. 3, the simulated BER is plotted versus the DC bias with 16-QAM for different values of E_b/N_0. It can be noticed that the curves have a minimum value at the optimal DC bias. Also, plotted in the same figure for comparison, is the analytical optimal DC bias given by (69) and the corresponding analytical BER. The simulation and analytical results closely agree.

IX. Simulation of Multipath Impulse Response for Indoor Wireless Optical Channels

In this section, we numerically evaluate the impulse response of an indoor wireless optical channel. In particular, we consider the indoor wireless optical channel with Lambertian reflectors. The channel model is described in detail in [16]. We use the same simulation parameters listed in Table I in [16] (Configuration A), except that we consider light rays making only up to one bounce, and the number of differential reflecting elements is decreased as follows:

$$\begin{aligned} N_x &= 25 \\ N_y &= 25 \\ N_z &= 15 \end{aligned} \tag{70}$$

The impulse response of the indoor wireless channel is plotted in Fig. 4. For a transmitted impulse having a power of 1 W, the line-of-sight (LOS) component power detected by the receiver is 1.23 W, which represents about 50% of the total power detected by the receiver if we consider up to 3 bounces from transmitter to receiver. Here, for simplicity, we consider only up to one reflection.

X. Simulation of ACO-OFDM in Indoor Wireless Optical Channels

In this section, we use the model developed in Section IX as the channel model in the simulation of an indoor wireless optical ACO-OFDM system. The simulation parameters are listed in Table I. A cyclic prefix (CP) is appended at the beginning of each OFDM frame. It consists of the last N_g samples of the OFDM frame. The CP serves as a guard interval, i.e. it eliminates the inter-symbol interference from the previous OFDM frame. More importantly for OFDM, using the CP, the linear convolution of a multipath channel is the same as circular convolution. Circular convolution in the time-domain is transformed to a simple multiplication in the frequency domain. This makes channel estimation and equalization easy provided the CP duration is larger than the duration of the channel impulse response. In the simulation, we assume perfect channel estimation and the equalization is done using a zero-forcing equalizer. The effect of the multipath indoor wireless optical channel on the system performance can be quantified from the comparison between the BER in the presence of AWGN only and the BER in the presence of AWGN and multipath. The BER performance for both cases is shown in Fig. 5. As expected, the multipath channel degrades the BER performane compared to the case of AWGN only.

TABLE I
ACO-OFDM Simulation Parameters

Parameter	Symbol	Value
Bandwidth	B	20 MHz
FFT Size	N	64
CP Length in Samples	N_g	4

XI. Conclusions

In this report, we have mathematically analyzed a DCO-OFDM system with the focus on the effect of the nonlinear clipping noise on the BER performance. Specifically, the clipping noise statistics were studied in detail, and an analytical formula was derived for use in the BER evaluation. The dependence of the BER on the DC bias, an important design parameter, is characterized in the BER formula. It can be seen that as the DC bias is increased, the transmitted power increases, but the nonlinear clipping noise is reduced leading to some sort of trade-off. Hence, the value of the DC bias should be optimized according to the system constraints and the required BER performance. In the light of this observation, we have found the optimal value of the DC bias, the one that minimizes the probability of error for a given E_b/N_0 and QAM constellation size M. Our analysis and results provide a theoretical basis for the design and implementation of DCO-OFDM systems. Our results are valid for wireless optical systems where the main source of noise is the electrical receiver front-end. Future work should consider optical fiber transmission and include the optical effects of chromatic dispersion, polarization mode dispersion, fiber nonlinearity, amplified spontaneous emission (ASE) noise, etc.

We also investigated ACO-OFDM which is less bandwidth-efficient than DCO-OFDM but more power-efficient. It is therefore more practical for applications requiring low power consumption. For example, in visible light communications, where the LEDs serve the function of lighting, in addition to communication, ACO-OFDM may be used to satisfy the dimming requirements while supporting communication at a lower bit rate than DCO-OFDM.

References

[1] J. B. Carruthers and J. M. Kahn. Multiple-subcarrier modulation for nondirected wireless infrared communication. *IEEE J. Sel. Areas Commun.*, vol. 14:pp. 538–546, 1996.

[2] O. Gonzalez, R. Perez-Jimenez, S. Rodriguez, J. Rabadan, and A. Ayala. OFDM over indoor wireless optical channel. *IEEE Proc. Optoelectronics*, vol. 152:pp. 199–204, 2005.

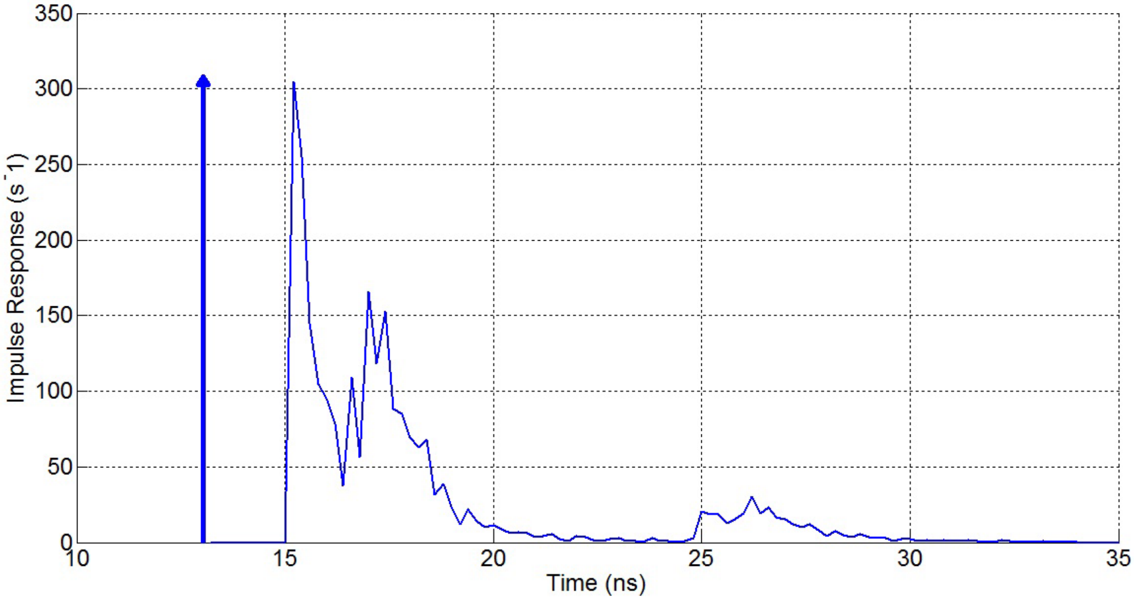

Fig. 4. Plot of the impulse response of the indoor wireless optical channel. Note that the unit impulse representing the LOS component is not drawn to scale.

[3] J. Armstrong and A. J. Lowery. Efficient optical OFDM. *Electron. Lett.*, vol. 42:pp. 370–371, 2006.

[4] J. Armstrong and B. J. C. Schmidt. Comparison of asymmetrically clipped optical OFDM and DC-biased optical OFDM in AWGN. *IEEE Commun. Lett.*, vol. 12:pp. 343–345, 2008.

[5] Jean Armstrong. OFDM for optical communications. *IEEE/OSA J. Lightwave Technol.*, vol. 27, no. 3:pp. 189–204, February 2009.

[6] D. Dardari, V. Tralli, and A. Vaccari. A theoretical characterization of nonlinear distortion effects in OFDM systems. *IEEE Trans. Communications*, vol. 48, no. 10:pp. 1755–1764, 2000.

[7] A. R. S. Bahai, M. Singh, A. J. Goldsmith, and B. R. Saltzberg. A new approach for evaluating clipping distortion in multicarrier systems. *IEEE J. Sel. Areas Commun.*, vol. 20, no. 5:pp. 1037–1046, Jun. 2002.

[8] H. Ochiai and H. Imai. Performance analysis of deliberately clipped OFDM signals. *IEEE Trans. Commun.*, vol. 50, no. 1:pp. 89–101, Jan. 2002.

[9] N. Y. Ermolova. Analysis of OFDM error rates over nonlinear fading channels. *IEEE Trans. Wireless Commun.*, vol. 9, no. 6:pp. 1855–1860, June 2010.

[10] A. Papoulis. *Probability, Random Variables, and Stochastic Processes*. New York: McGraw-Hill, 3rd edition, 1991.

[11] H. E. Rowe. Memoryless nonlinearities with Gaussian inputs: Elementary results. *Bell Syst. Tech. J.*, vol. 61, no. 7:pp. 1519–1525, Sept. 1982.

[12] J. Minkott. The role of AM-to-PM conversion in memoryless nonlinear systems. *IEEE Trans. Commun.*, vol. COM-33:pp. 139–144, Feb. 1985.

[13] X. Yi, W. Shieh, and Y. Ma. Phase noise effects on high spectral efficiency coherent optical OFDM transmission. *IEEE Journal of Lightwave Technology*, vol. 26, no. 10:pp. 1309–1316, May 2008.

[14] Svilen Dimitrov and Harald Haas. On the clipping noise in an ACO-OFDM optical wireless communication system. In *GLOBECOM*, pages 1–5, 2010.

[15] F.R. Gfeller and U. Bapst. Wireless in-house data communication via diffuse infrared radiation. *Proceedings of the IEEE*, 67(11):1474–1486, 1979.

[16] J.R. Barry, J.M. Kahn, W.J. Krause, E.A. Lee, and D.G. Messerschmitt. Simulation of multipath impulse response for indoor wireless optical channels. *Selected Areas in Communications, IEEE Journal on*, 11(3):367–379, 1993.

[17] J.M. Kahn and J.R. Barry. Wireless infrared communications. *Proceedings of the IEEE*, 85(2):265–298, 1997.

[18] Y. Tanaka, T. Komine, S. Haruyama, and M. Nakagawa. Indoor visible communication utilizing plural white LEDs as lighting. In *Personal, Indoor and Mobile Radio Communications, 2001 12th IEEE International Symposium on*, volume 2, pages F–81–F–85 vol.2, 2001.

[19] M. Akanegawa, Y. Tanaka, and M. Nakagawa. Basic study on traffic information system using LED traffic lights. *Intelligent Transportation Systems, IEEE Transactions on*, 2(4):197–203, 2001.

[20] T. Komine and M. Nakagawa. Integrated system of white LED visible-light communication and power-line communication. *Consumer Electronics, IEEE Transactions on*, 49(1):71–79, 2003.

[21] S.-H. Yang, E.-M. Jeong, D.-R. Kim, H.-S. Kim, Y.-H. Son, and S.-K. Han. Indoor three-dimensional location estimation based on LED visible light communication. *Electronics Letters*, 49(1):54–56, 2013.

[22] S. Hranilovic and F.R. Kschischang. A pixelated MIMO wireless optical communication system. *Selected Topics in Quantum Electronics, IEEE Journal of*, 12(4):859–874, 2006.

[23] T. Komine and M. Nakagawa. Fundamental analysis for visible-light communication system using LED lights. *Consumer Electronics, IEEE Transactions on*, 50(1):100–107, 2004.

[24] Raed Mesleh, Hany Elgala, and Harald Haas. On the performance of different OFDM based optical wireless communication systems. *J. Opt. Commun. Netw.*, vol. 3, no. 8:pp. 620–628, August 2011.

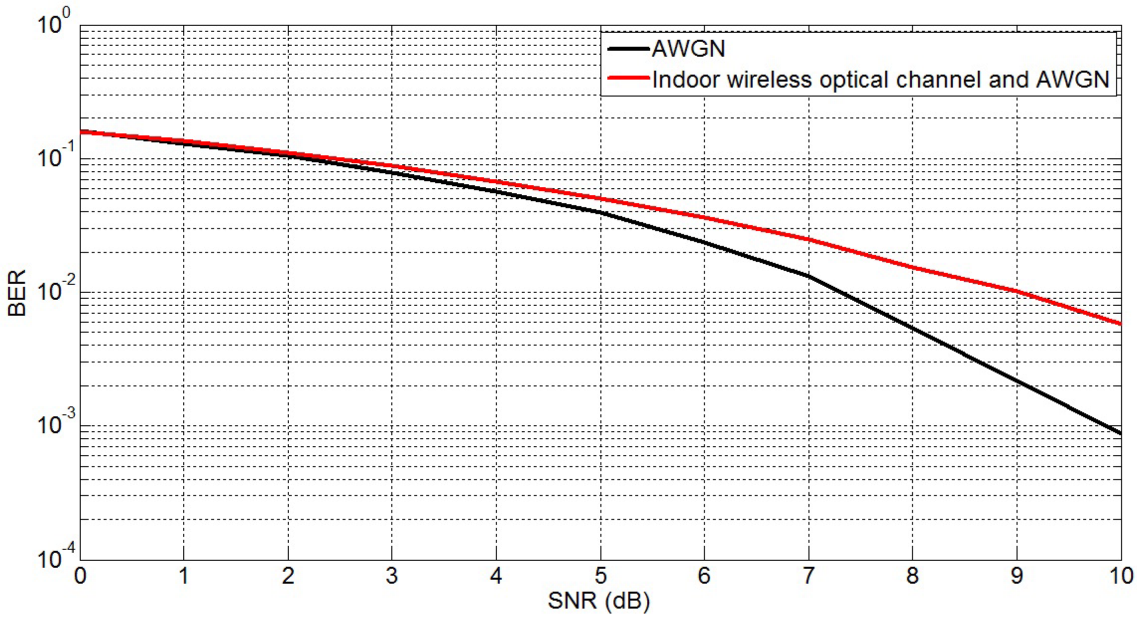

Fig. 5. BER curves for ACO-OFDM in (a) AWGN only (black) and (b) multipath indoor wireless optical channel and AWGN (red).